Semi-Adaptive Beamforming for OFDM based Hybrid Terrestrial-Satellite Mobile System

Ammar H. Khan, *Student Member, IEEE,* Muhammad A. Imran, *Member, IEEE,* and Barry G. Evans, *Senior Member, IEEE*

Abstract

Adaptive interference mitigation requires significant resources due to recursive processing. Specific to satellite systems, interference mitigation by employing adaptive beamforming at the gateway or at the satellite both have associated problems. While ground based beamforming reduces the satellite payload complexity, it results in added feeder link bandwidth requirements, higher gateway complexity and suffers from feeder link channel degradations. On the other hand, employing adaptive beamforming onboard the satellite gives more flexibility in case of variation in traffic dynamics and also for changing of beam patterns. However, these advantages come at the cost of additional complexity at the satellite. In pursuit of retaining the benefits of onboard beamforming and to reduce the complexity associated with adaptive processing, we here propose a novel semi-adaptive beamformer for a Hybrid Terrestrial-Satellite Mobile System. The proposed algorithm is a dual form of beamforming that enables adaptive and non-adaptive processing to coexist via a robust gradient based switching mechanism. We present a detailed complexity analysis of the proposed algorithm and derive bounds associated with its power requirements. In the scenarios studied, results show that the proposed algorithm consumes up to 98% less filter computing power as compared to full-adaptive case without compromising on system performance.

Index Terms

OFDM, Beamforming, LMS, Semi-Adaptive, Hybrid

The authors are with the Centre for Communication Systems Research (CCSR), University of Surrey, Guildford GU2 7XH, U.K. (e-mail: a.h.khan@surrey.ac.uk).

I. Introduction

Advanced signal processing and Orthogonal Frequency Division Multiple Access (OFDM) technology offers a comprehensive solution towards future high capacity networks. In conjunction with high capacity, networks must also offer ubiquitous service. Following this objective, we proposed an OFDM based Hybrid Terrestrial-Satellite Mobile System (HTSMS) [1].

In HTSMS, the nature of hybrid architecture causes considerable increase in uplink Co-Channel Interference (CCI) and thus adaptive interference mitigation becomes imperative [2]. Hence to mitigate uplink CCI in [1], we employ Least Mean Squares (LMS) based adaptive Beamforming (BF) at the satellite. BF has been studied in detail with reference to OFDM [3]–[5]. For the hybrid system, we have previously proposed several adaptive BF strategies [6]–[8].

The implementation of onboard BF will increase the satellite mass, power as well as the associated costs. However with advancement of technology as predicted by Moore's law, BF and other resource intensive operations can potentially be implemented onboard the satellite by having onboard digital processing in future. To highlight advancements in satellite payload, Inmarsat-4 satellites (2005) have 6 times more power, 3 times larger solar array and 4 times dry mass as compared to Inmarsat-2 (1990). Following similar trend, future satellite may well have sophisticated payload design, having features such as a reprogrammable architecture.

To reduce satellite payload complexity, current generation of satellite systems such as ICO [9], SkyTerra [2] employ Ground Based Beamforming (GBBF) with full adaptivity. GBBF is at present the most convenient and cost effective BF approach as it keeps the satellite complexity to the minimum. It however requires a large amount of transceiver hardware and bandwidth for gateway uplink/downlink communications. To address the trade-off between onboard and ground BF, recently hybrid onboard/ground BF solutions [10], [11] have been proposed where some parts of the BF processes are done onboard and some at the gateway. This hybrid approach where BF is split can be viewed as a form of compression since received feed signals are

projected on a subspace to reduce the required feeder link bandwidth. In addition to this, further compression techniques can be envisioned to reduce the bandwidth requirement of both GBBF and hybrid approaches. However we examine this trade-off from a different perspective. The main motivation behind aforementioned hybrid topologies is to reduce 1) the complexity onboard the satellite and 2) feeder link bandwidth. The more we move towards the space BF approach, the feed requirements reduces but complexity onboard the satellite increases. If, however, we can develop power efficient BF mechanisms, we could simultaneously achieve both objectives.

To reduce the complexity of adaptive filtering, partial update of LMS algorithms has been proposed [12]–[14] where a only subset of filter coefficients are updated. Complexity reduction can also be achieved by processing a subspace of the received signal [15], [16]. As oppose to aforementioned approaches, we propose a novel semi-adaptive beamformer for HTSMS scenario to achieve complexity reduction. The proposed technique is a dual onboard beamformer which switches between adaptive and non-adaptive processing depending on the received signal characteristics. As compared to full-adaptive BF, the switching-off feature enables reduced BF filter computing power when not required. We develop a novel gradient based switching mechanism which enables adaptive and non-adaptive processing to coexist. Moreover, the proposed BF algorithm is shown to be robust to disturbances in the system as well as to spurious switching.

The following notations will be used throughout the paper. $\mathbf{A}$ and $\tilde{\mathbf{A}}$ denote a matrix in the time and frequency-domain respectively, whereas $\mathbf{a}$ represents a vector. $[\mathbf{A}]_{n,m}$ represents an element at the n^{th} row and m^{th} column of $\mathbf{A}$.

II. Hybrid Terrestrial-Satellite Mobile System Model

A. HTSMS Scenario

The HTSMS aims to provide global coverage and higher capacity by integrating satellite and terrestrial networks. In essence, users in rural areas are served by the satellite link whereas urban area users are served by terrestrial cellular Base Stations (BTSs). Terrestrial and satellite networks

both reuse their spectrum resulting in increased overall capacity. Similar hybrid topologies have also been employed by DVB-SH [17] and SkyTerra [18] where they use Complimentary Ground Component (Europe) or Ancillary Terrestrial Component (U.S.) as terrestrial gap-fillers.

Fig. 1 depicts the HTSMS and hybrid scenario. Due to frequency reuse, CCI is induced by the terrestrial users on the uplink of a Geostationary (GEO) satellite. This is mitigated using onboard Pre-FFT adaptive BF based on LMS filtering. Other variants of LMS can also be adopted such as NLMS [19], [20] and VSS-LMS [21] that provide better convergence, which we have implemented in our previous work [7]. Recursive Least Squares (RLS) can also be employed which offers an order faster convergence than LMS. This however comes at the cost of complexity; LMS requires $2M$ multiples per update whereas RLS requires $4M^2 + 4M + 2$ multiples per update [22]. Furthermore, RLS suffers from slower convergence at low SNR levels.

We employ OFDM on the uplink in the return direction. Traditionally OFDM has not been the air interface choice in the return link. However recently ETSI MSS forum has initiated standardization for the return link of DVB-SH, named S-band Mobile Interactive Multimedia (S-MIM), to provide satellite access to the users in the return direction with OFDM as a potential candidate. Similarly on the terrestrial front, LTE-A has opted for OFDM as the air interface for the return link. The trend indicates an increasing use of OFDM and therefore we employ OFDM.

In HTSMS, a mobile and satellite link is modelled as Single Input Multiple Output (SIMO). A Uniform Linear Array (ULA) of S antenna elements is modelled at the satellite. Total J users operate with one desired user d being served by satellite and the rest being interferers served by BTSs. After the signal is received, BF is applied onboard the satellite to mitigate CCI. The interference model and geometry of users' Direction-of-Arrival (DOA) is illustrated in Fig. 1.

OFDM is susceptible to Carrier Frequency Offsets (CFO) [23], which causes sub-carrier non-orthogonality. This raises Inter Carrier Interference (ICI). As we focus on CCI mitigation, we assume the Radio Access Network (RAN) employs timing and CFO estimation and recovery [24]. However in this paper we do investigate the impact of CFO on system's throughput.

B. OFDM Transmitter Model for HTSMS

Fig. 2 is the transceiver architecture of the Bit Interleaved Coded Modulation (BICM)-OFDM based HTSMS and will be referred to throughout the paper to follow the information flow. Binary information bits $\{\mathbf{o}\}$ are generated by the j^{th} user terminal, which are encoded into $\{\mathbf{t}\}$ and then interleaved into $\{\mathbf{c}\}$. Interleaved bits $\{\mathbf{c}\}$ are then mapped into QPSK complex symbols and Serial-to-Parallel (S/P) converted to $\{\widetilde{\mathbf{x}}^q\}$. Pilots $\{\widetilde{\mathbf{x}}^p\}$ are interspersed into data sequence $\{\widetilde{\mathbf{x}}^q\}$ at known pilot sub-carriers $\{\mathscr{I}\}$. The process outputs N sub-carrier OFDM symbol that can be expressed as:

$$\widetilde{\mathbf{x}}_j = [\widetilde{x}_j(0), \widetilde{x}_j(1), \ldots, \widetilde{x}_j(N-1)]^T \quad . \qquad j = 1, \ldots, J \quad . \tag{1}$$

For the sake of brevity, we drop the subscript j that indicates user indexing. After formation of OFDM symbol, $\widetilde{\mathbf{x}}$ is converted to the time-domain by a N-point IFFT which is given by:

$$\mathbf{x} = \mathbf{F}^H \widetilde{\mathbf{x}} \ , \tag{2}$$

where

$$\mathbf{F} = \begin{bmatrix} 1 & 1 & \cdots & 1 \\ 1 & e^{-j2\pi(1)(1)/N} & \cdots & e^{-j2\pi(1)(N-1)/N} \\ \vdots & \vdots & \ddots & \vdots \\ 1 & e^{-j2\pi(N-1)(1)/N} & \cdots & e^{-j2\pi(N-1)(N-1)/N} \end{bmatrix} \ . \tag{3}$$

The start of every OFDM symbol is appended by a CP of length G. The output $\bar{\mathbf{x}} = [x(-G), x(-G+1), \ldots, x(N-1)]^T$ is serially transmitted over the channel, whose effect can be presented as:

$$\bar{\mathbf{y}}[k] = \bar{\mathbf{x}}[k] \otimes \mathbf{h}[k] \ . \tag{4}$$

C. BICM-OFDM Receiver Layout

The signals from desired and interference sources are received at the satellite antenna elements. The ULA output after CP removal for the l^{th} OFDM symbol ($l = 1, \ldots, L$) is given by:

$$\mathbf{V} = \mathbf{A}\mathbf{Y}^H + \mathbf{B} \ , \tag{5}$$

where $[\mathbf{Y}]_{n,j}$ is the received n^{th} sub-carrier for the j^{th} user. Similarly $[\mathbf{B}]_{s,n}$ and $[\mathbf{V}]_{s,n}$ represents the independent and identically distributed (i.i.d) complex Gaussian noise $\sim \mathscr{CN}(0, \sigma^2)$ and ULA output at the s^{th} antenna element and n^{th} sub-carrier respectively, where $s = 1, \ldots, S$ is the array element index of the ULA. $\mathbf{A}$ is the ULA response, where $[\mathbf{A}]_{s,j}$ can be presented as:

$$a(s, j) = e^{(-j2\pi(s-1)d_a \sin(\theta_j)/\lambda)} \ . \tag{6}$$

$d_a = \lambda/2$ is the inter-antenna element spacing, θ_j is the Direction-Of-Arrival (DOA) of the j^{th} user and λ is the carrier wavelength. $\mathbf{V}$ is processed by the beamformer, which is given as:

$$\mathbf{z} = \mathbf{w}^H\mathbf{V} \ , \tag{7}$$

where $\mathbf{z} = [z(0), z(1), \ldots, z(N-1)]$ is the weighted output of the beamformer and $\mathbf{w} = [w(1), w(2), \ldots, w(S)]^T$ are the applied BF complex weights. $\mathbf{z}$ is S/P converted and transformed to the frequency-domain, which can be expressed as:

$$\widetilde{\mathbf{z}} = \mathbf{F}(\mathbf{w}^H\mathbf{A}\mathbf{Y}^H + \mathbf{w}^H\mathbf{B})^H \ . \tag{8}$$

In AWGN channel case, data sub-carriers in $\widetilde{\mathbf{z}}$ are de-multiplexed into $\widetilde{\mathbf{r}}^q$ and then passed to QPSK demapper. In case of fading channel, Channel Estimation (CE) is performed on $\widetilde{\mathbf{z}}$ to yield $\widetilde{\mathbf{r}}$ which is then de-multiplexed into $\widetilde{\mathbf{r}}^q$. Demapper computes *a posteriori* probability (APP) given received vector $\widetilde{\mathbf{r}}^q$ and channel estimates $\widetilde{\mathbf{h}}^q$. It outputs *extrinsic* information or Log-Likelihood

Ratio (LLR) Γ for the v^{th} coded bits c_v in the desired user's transmitted data sequence $\widetilde{\mathbf{x}}_d^q$.

$$\Gamma(c_v(\tilde{x}_d^q(n))) = \ln \frac{\sum_{b \in U_v^+} P(\tilde{x}_d^q(n) = b \mid \tilde{r}^q(n), \tilde{h}^q(n))}{\sum_{b \in U_v^-} P(\tilde{x}_d^q(n) = b \mid \tilde{r}^q(n), \tilde{h}^q(n))} \ , \tag{9}$$

$$P(\tilde{x}_d^q(n) = b \mid \tilde{r}^q(n), \tilde{h}^q(n)) = \frac{1}{2\pi\sigma^2} \exp(-\frac{\|\tilde{r}^q(n) - \tilde{h}^q(n)\tilde{x}_d^q(n))\|^2}{2\sigma^2}) \ , \tag{10}$$

where U_v^- and U_v^+ is the constellation set containing all the symbols whose v^{th} bit is 0 and 1 respectively. The LLRs of the coded bits are de-interleaved and passed to the MAP decoder which outputs the decoded bits $\{\hat{\mathbf{o}}\}$. For the next symbol, LMS computes new BF weights which takes the error between desired user's transmitted and received pilot sequence as an input.

$$\widetilde{\mathbf{e}} = \widetilde{\mathbf{z}}^p - \widetilde{\mathbf{x}}_d^p \ . \tag{11}$$

As we employ Pre-FFT BF, $\widetilde{\mathbf{e}}$ is converted to the time-domain which can be presented as:

$$\mathbf{e} = \mathbf{F}^H \widetilde{\mathbf{e}} \ . \tag{12}$$

D. Full-Adaptive Beamformer

The LMS algorithm recursively computes BF weights based on the error vector $\mathbf{e}$ until all data has been decoded. The LMS adaptation is given by:

$$\mathbf{w}[l+1] = \mathbf{w}[l] + 2\mu \mathbf{V}[l]\mathbf{e}[l] \tag{13}$$

where $\mathbf{w}[l]$ and $\mathbf{w}[l+1]$ represent the BF complex weights for l and $l+1$ OFDM symbol. μ represents the step size which controls the rate of convergence. The algorithm only converges [21]:

$$\mu_{min} \leq \mu \leq \mu_{max} \ , \qquad \mu_{min} > 0 \ , \tag{14}$$

$$\mu_{max} \leq \frac{2}{3\,\mathrm{tr}\,(\mathbf{R})} \ . \tag{15}$$

When constant μ is employed with LMS, μ will be close to μ_{min} to provide minimum tracking capability.We employ LMS with optimised μ that adapts at each iteration according to (15).

III. Proposed Semi-Adaptive Beamformer

A. Algorithm Formulation

LMS is driven by energy of instantaneous errors $e[k]$ and the desired user signal $d[k]$:

$$e[k] = d[k] - \mathbf{x}^T[k]\mathbf{w}[k] \ . \tag{16}$$

$$d[k] = \mathbf{x}^T[k]\mathbf{w}^*[k] + \delta[k] \ . \tag{17}$$

Here $\mathbf{x}[k]$, $\mathbf{w}[k]$ and $\delta[k]$ are the received signal, BF weights and the error floor at time instance $[k]$ respectively. By substituting (17) into (16), we obtain:

$$\begin{aligned} e[k] =& \mathbf{x}^T[k](\mathbf{w}^*[k] - \mathbf{w}[k]) + \delta[k] \ , \\ =& \varepsilon[k] + \delta[k] \ , \end{aligned} \tag{18}$$

where $\varepsilon[k]$ is the random error. For the conventional full-adaptive LMS, $e[k]$ is used to recursively adapt $\mathbf{w}[k]$ leading to consistent reduction in $e[k]$. In an ideal case when $\delta[k] = 0$:

$$\lim_{k\to\infty} e[k] \to 0 \ . \tag{19}$$

In the ideal environment, state (19) would be achieved indicating perfect interference mitigation which can be used to switch-off adaptive BF. However $\delta[k]$ persists due to system noise and $e[k]$ fluctuates around its mean and hence is not stable. Therefore, $e[k]$ cannot be used as an appropriate Beamforming Switching Metric (BSM). With the objective to derive a suitable BSM, if we denote ω_l as the Mean Squared Error (MSE) of the l^{th} OFDM symbol, then the variance of ω_l can be given as:

$$\Psi_{L-1} = \frac{1}{L-1}\sum_{l=1}^{L-1}(\omega_l - \bar{\omega})^2 + \acute{\delta} \ , \tag{20}$$

where $\acute{\delta}$ is the variance floor. Variance Ψ_{L-1} is computed over a Monitoring Window (MW) of $L-1$ symbols whose size incrementally grows from 1 to $L-1$. When the L^{th} OFDM symbol is received, the variance over $\parallel$ MW $\parallel = L$ as a function of ω_l and (20) is given as:

$$\Psi_L = \frac{1}{L}((L-1)\Psi_{L-1} + (\omega_l - \bar{\omega})^2 + \acute{\delta}) \ . \tag{21}$$

The gradient between (21) and (20) as a function of Ψ_{L-1} and Ψ_{L-2} can be formulated as:

$$\nabla\Psi_L = \frac{(L-1)^2\Psi_{L-1} - L(L-2)\Psi_{L-2} + (L-1)(\omega_l - \bar{\omega})^2 + L(\omega_{l-1} - \bar{\omega})^2}{L(L-1)} \ . \tag{22}$$

$$\lim_{L\to\infty} \nabla\Psi_L \to 0 \ . \tag{23}$$

As $\nabla\Psi_L$ is independent of the variance floor $\acute{\delta}$ and $\nabla\Psi \to 0$ irrespective of the $\acute{\delta}$, ω_l and $\bar{\omega}$, hence it can be used as a BSM. Moreover as $\nabla\Psi$ is measured over a MW, it is more reliable as compared to $e[k]$. However, we also note in (22) that when $\parallel$ MW $\parallel \to \infty$ ($L \to \infty$), then:

$$\lim_{L\to\infty} \frac{(\omega_l - \bar{\omega})^2 + (\omega_{l-1} - \bar{\omega})^2}{L} \to 0 \ . \tag{24}$$

In other words when L is large, $\nabla\Psi$ is insensitive to changes in the input signal $\mathbf{x}$. With respect to BF, this makes the BSM immune to changes in the interference profile. To solve this, we define a Moving Monitoring Window (MMW) such that:

$$\parallel \text{MMW} \parallel = \rho \ . \qquad \rho \ll \infty \ . \tag{25}$$

In generic form, MMW moves over g symbols while performing continuous monitoring of $\nabla\Psi$. Now with the MMW, state (24) can be reformulated as:

$$\lim_{L\to\rho} \frac{(\omega_l - \bar{\omega})^2 + (\omega_{l-1} - \bar{\omega})^2}{L} \nrightarrow 0 \ . \tag{26}$$

With MMW, $\nabla\Psi$ will respond if characteristics in $\mathbf{x}$ change. Moreover, $L \nrightarrow \infty$ implies $\nabla\Psi_L \nrightarrow 0$ and would vary within given bounds. Now to derive these bounds we assume for simplicity the return link to be AWGN. Hence for $\sim \mathscr{CN}(0, \sigma^2)$, the variance of the mean of $\nabla\Psi$ is:

$$\Omega = \text{Var}\left(\frac{1}{\rho}\sum_{l=1}^{\rho}\nabla\Psi_l\right) \quad . \tag{27}$$

As all variables have the same variance σ^2, division by ρ becomes a linear transformation. Hence:

$$\Omega = \frac{\sigma^2}{\rho} \quad . \tag{28}$$

We observe that if $\rho \to \infty$, then $\Omega \to 0$ which is consistent with (23). With respect to BF, imposing MMW will result in $\nabla\Psi$ varying within the bound derived in (28). This is given by:

$$\mid \nabla\Psi \mid \leq \mid \Omega \mid \quad . \tag{29}$$

The state (29) is achieved after BF convergence. $\nabla\Psi$ provides switching functionality while taking into account changes in the system. However in a practical BSM enabled BF system, there is a probability of False Switching (FS) and hence the switching mechanism should be stable and robust. To ensure this, we monitor $\nabla\Psi$ over a Moving Monitoring Block (MMB) of f consecutive MMWs which slides over g symbols. When all f MMWs meet the criteria in (29), a Beamforming Triggering Flag (BTF), denoted by Λ, is set to 0 causing a switch from adaptive to non-adaptive BF. If at any time after the switch, all f MMWs violate the criteria in (29), adaptive BF is switched back on by setting Λ to 1. The selection of f is a trade-off between different criteria. A large f means more robustness, but this is at the cost of 1) increased delay before a switch can be triggered 2) increased computation requirement and 3) reduced responsiveness to instantaneous changes. Algorithm 1 is the pseudo-code representation of the proposed approach.

To verify the algorithm's working, Fig. 3 presents $\nabla\Psi$ with MW and MMW. For the case of MW ($L = \infty$), $\nabla\Psi = 0$ for $l \geq 200$, which is consistent with (23). As L increases, no fluctuation

is observed in $\nabla\Psi$, which is again consistent with (24). On the other hand for the MMW case with $\rho = 50$, $\nabla\Psi$ is within the bounds after $l \approx 125$. Interestingly we also observe that $\nabla\Psi$ is not a constant value with increase in L and at all times $\mid \nabla\Psi \mid \leq \mid \Omega \mid$. This verifies (26) and that MMW topology is able to track changes in the system. Hence for this particular scenario, we can potentially trigger the switch when $l = 150$. However with MMB and for instance $f = 3$, $\nabla\Psi$ monitoring will continue for at least $l \geq 250$. The advantage of using the MMB approach is hence twofold, 1) it ensures the algorithm is stable and robust towards FS and 2) by defining f, we can optimise the number of symbols prior to which a switch cannot be triggered, thus:

$$L_{min} = \rho \times f \tag{30}$$

B. Semi-Adaptive Operation

Initially BF weights are adapted according to (12)−(13). When criteria in (29) over a MMB is met, Λ is set to 0. This triggers non-adaptive BF which is given by:

$$\mathbf{w}[l+1] = \mathbf{w}[l]. \tag{31}$$

In terms of OFDM symbols, the switch triggering point is denoted as L_s. After this if at any time the criteria in (29) is violated over a MMB, Λ is set to 1 triggering reversal to adaptive BF.

IV. Complexity Analysis of Semi-Adaptive against Full-Adaptive BF

The complexity of full-adaptive BF (Section II-D) can be presented as:

$$\beta_A = LS(M + N(M + P)) \qquad \forall L \ , \tag{32}$$

where M and P represent multiplication and addition operations respectively. The semi-adaptive algorithm has an adaptive BF phase, similar to (32). The monitoring phase of the algorithm does computation of 1) variance Ψ 2) gradient $\nabla\Psi$ 3) threshold Ω and 4) switching decision. For the

MMB processing, these factors with the aim of minimising M can be expressed as:

$$\begin{aligned}\beta_{SA} = & \overbrace{\beta_{A'}}^{AdaptiveBF} + \overbrace{\beta_{\Psi}+\beta_{\nabla\Psi}+\beta_{s}+\beta_{\Omega}}^{Monitoring} \quad . \\ & = [L_s S(M+N(M+P))] + \\ & \left[\left(\frac{L}{\rho}\right)\times\{4M+(\rho+2)\,P\}\right] + \\ & \left[2P+(f-2)\{M+P\}+\left(\frac{L-f\rho}{g}\right)P+\left(\frac{L-f\rho}{\rho}\right)\{M+P\}\right] + \\ & \left[\left(\frac{L-f\rho}{g}+1\right)P\right] + \\ & [\gamma_s M] \quad .\end{aligned} \tag{33}$$

Proof of (33) is presented in Appendix A. Here γ_s is the number of times Ω in (28) is re-evaluated due to change in system noise. If the available SNR does not change, Ω will be computed once, as in our case ($\gamma_s = 1$). With this assumption, we split (32), (33) into M and P components:

$$\beta_A^m = M\,[LS(1+N)] \quad . \tag{34}$$

$$\beta_A^p = P\,[LSN] \quad . \tag{35}$$

$$\beta_{SA}^m = M\left[L_s S(1+N)+\frac{5L}{\rho}-1\right] \quad . \tag{36}$$

$$\beta_{SA}^p = P\left[L_s SN+\frac{3L+\rho L}{\rho}+\frac{2(L-f\rho)}{g}+1\right] \quad . \tag{37}$$

Now using (34)$-$(37), we define the potential gain $\hbar$ as the relative BF filter computing power consumed by semi-adaptive BF algorithm if 1 unit is expended by the full-adaptive case:

$$\hbar = \left(\frac{\beta_{SA}^m}{\beta_A^m+\beta_A^p}+\frac{\beta_{SA}^p}{\beta_A^m+\beta_A^p}\right) \quad , \tag{38}$$

***Lemma 1*:** M operations are a factor f_m more complex than P.

We assign a factor f_m to P such that $M = f_m P$. Now substituting (34)−(37) into (38):

$$\hbar = \left(\frac{f_m \left[\frac{L_s(1+N)}{L} + \frac{5}{\rho S} - \frac{1}{LS} \right] + \left[\frac{L_s N}{L} + \frac{3+\rho}{\rho S} + \frac{2(L-f\rho)}{gLS} + \frac{1}{LS} \right]}{f_m \left[1+N\right] + \left[N\right]} \right) \quad . \tag{39}$$

***Lemma 2*:** M operations are far more complex than P, hence assume $\frac{1}{fm} = 0$.

$$\begin{aligned} \hbar^{m_1} =& \frac{\frac{L_s(1+N)}{L} + \frac{5}{\rho S} - \frac{1}{LS}}{(1+N)} \quad . \\ =& \frac{L_s}{L} + \left(\frac{5}{\rho S(1+N)} - \frac{1}{LS(1+N)} \right) \quad . \end{aligned} \tag{40}$$

***Lemma 3*:** L is a large number, hence $\frac{1}{LS(1+N)} \approx 0$.

$$\hbar^{m_2} = \frac{L_s}{L} + \frac{5}{\rho S(1+N)} \quad , \tag{41}$$

***Lemma 4*:** $\rho S((1+N)) \gg 5$.

$$\hbar^{'} \approx \frac{L_s}{L} \quad . \tag{42}$$

$\hbar^{'}$ in (42) and $\hbar$ in (39) is the minimum and maximum BF filter computing power consumption respectively of the semi-adaptive case as compared to full-adaptive BF. We have assumed in the complexity analysis that the switching takes place once, or in other words the interference scenario is stationary as such and the system is stable. In practise, the switching may take place more than once and hence reducing the computation gain. However the interference dynamics in a satellite scenario are far more subtle as compared to terrestrial environment. For instance, if a user moves with 60 km/hr velocity for 1 hr, then the rate of change of DOA with respect to a GEO satellite is $\sim 0.0016^{\circ}/$min. In comparison, if the same user moves in circular motion at the cell edge of a cellular BTS having cell radius of 3 km, the rate of change comes out as $\sim 19.1^{\circ}/$min. Hence it is safe to assume that the switching operations will be on a far less frequent basis which will result in potentially higher gain as compared to full-adaptive BF.

V. Simulation and Discussions

A. Simulation Parameters

A SIMO BICM-OFDM system with 32 sub-carriers (N) having 5 pilots per symbol (N_p) is modelled. 1×2 and 1×4 SIMO configurations are employed. In accordance with Fig. 1, one desired user is modelled at 40° while interferers at -70°,-35° and 60° azimuth respectively. Total OFDM symbols transmitted (L) $= 40,000$. A rate-$1/2$ $(5,7)_8$ convolution encoder and random interleaver/de-interleaver are employed. The power per interferer at the satellite end is -5 dBW, whereas of the desired user is 0 dBW. Transmission frequency is taken as 3 GHz.

B. Semi-Adaptive Switching

First we analyse the switching functionality of the algorithm. Fig. 4 presents the absolute Real-time Beamforming Weights (RBFW) of one of the antenna elements for $\sigma^2 = 1.0$ & 0.16. For the case of higher noise ($\sigma^2 = 1.0$), we note that the semi-adaptive algorithm switches off adaptive BF when $l = 650$ and weights are frozen hereafter. With $\sigma^2 = 0.16$, switch takes place when $l = 500$ due to lesser disturbance. Hence with lower noise level, the proposed algorithm initiates the switch much earlier as compared to the case with high noise. Furthermore, the switch takes place when $l \geq 500$ OFDM which verifies (30) as $L_{min} = 500$ using ρ and f in (30).

C. Computational Gain

Prior to investigating the system performance, we first determine how much computational saving can be achieved using (39)$-$(42). Employing $S = 4$ and for the case $\sigma^2 = 1$, the switch is triggered with $L_s = 650$. The minimum relative BF filter computation power consumption (*lemma 4*) for this case is 0.0163 and if we also include MMB processing (*lemma 1 - 3*), the consumption increases to 0.0177. This effectively means significant saving of resources as the semi-adaptive algorithm switches off adaptive BF while using minimum energy during MMB processing. When noise reduces with $\sigma^2 = 0.16$, the switch is triggered earlier and $L_s = 500$. This further reduces

the BF filter computing power consumption with minimum consumption of 0.0125 and maximum of 0.0139. With $L_s = 650$, the semi-adaptive requires 98.23% lesser computational power as compared to full-adaptive. Moreover, when $L_s = 500$ the gain increases to 98.67%. Hence irrespective of the noise level, the semi-adaptive is far less complex as compared to the full-adaptive case. It must be noted that our analysis does not consider power consumption of other components and reported performance only relates to reduction in BF filter computation.

D. System Performance

We have seen so far that the proposed algorithm shows promise in terms of computation saving. Now to establish the benefits of the proposed algorithm, we need to compare its performance against the full-adaptive case. Hence, Fig. 5 presents the MSE (BF prediction error) performance of adaptive and proposed semi-adaptive beamformer against E_b/N_o. For the case of $S = 2$, we see that the performance of both the schemes is almost identical. When the number of antenna elements are increased to 4, we see that up to $E_b/N_o = 4$ dB the MSE curves for both the schemes overlap. Beyond this, a slightly better performance from the full-adaptive case is observed. At 8 dB E_b/N_o, the semi-adaptive beamformer's performance is degraded by only 0.37 dB.

The 0.37 dB is such a minimal degradation that it would inevitably have almost no effect on the Bit Error Rate (BER) performance. In order to verify this hypothesis, we compare the system performance in terms of BER in Fig. 6. Interestingly we can see that irrespective of the available E_b/N_o or the antenna elements employed, the semi-adaptive performance is almost identical to the full-adaptive case. Moreover, the general trend observed is consistent with previous results i.e. improved BER with higher E_b/N_o and with more antenna elements. This result is encouraging as it can pave the way for efficient adaptive processes on an "*if and when*" required basis.

E. Impact of CFO

Now we consider CFO in the system which arises ICI and analyse its impact on the system's throughput. Focusing on the return link, we compute throughput while considering typical MSS parameters depicted in Table II. The analysis is based on a realistic assumption that Satellite-to-Hub link has the lowest available C/N_o. Based on the MSS parameters, the throughput for different target BERs is plotted in Fig. 7 for the case of No CFO and with CFO in the system. We can see that CFO can cause considerable reduction in the available throughput if not compensated. For the specified target BERs, throughput reduces to $\sim$50$\%$ when ICI due to CFO increases to 3 dB. As OFDM is susceptible to CFO, hence its compensation becomes very critical.

F. Impact of Channel Fading

Finally we look at how removing the "*Gaussian*" assumption impacts the semi-adaptive operation and the system performance. We model the return link as multi-path time selective channel with parameters specific to the terrestrial-satellite scenario. The multi-path phenomenon is modelled as a linear Finite Impulse-Response (FIR) filter and the time selectivity using Jakes model. The channel parameters considered were measured as part of the EU project MAESTRO [25] and we consider Outdoor Rural case of MAESTRO which is presented in Table III. Now due to the incorporation of channel fading, Ω must be remodelled to capture the spread in the signal variation. Hence if h_l are the channel estimates for the l^{th} symbol, then:

$$\begin{aligned} \Omega &= \Omega_{Noise} + \Omega_{Fading} \ , \\ \Omega &= \Omega_{\sigma^2} + \text{std}(\mid h_l \mid) \ , \end{aligned} \tag{43}$$

where std$\{\}$ represents standard deviation. We employ Least Squares (LS) channel estimation for computing h_l. Due to the presence of channel fading on top of interference and noise during the BF convergence phase, we do not start the monitoring process from the very first OFDM symbol. The monitoring/switching phase is deferred by a total L_c symbols to ensure BF convergence.

With this in mind, Fig. 8 presents $\nabla\Psi$ vs OFDM symbols. We can observe that after initial convergence phase, $\nabla\Psi$ varies within the bounds which means switching can be performed. After verifying the bounds, now we present the BER performance of the proposed algorithm for the MAESTRO channel case in Fig. 9 for mobile speed of 3 km/hr. We can observe that BER performance of the semi-adaptive algorithm is almost the same as the full-adaptive case for both antenna element configurations. However as we have introduced L_c and monitoring of the channel estimates, the computation gain provided by the semi-adaptive algorithm will reduce.

VI. Conclusion

We have proposed here a novel semi-adaptive beamformer that is based on a novel switching mechanism. The approach enables sleep/awake procedures for adaptive interference mitigation by employing beamforming "*if and when*" required thus making it more energy efficient as compared to the full-adaptive case. The switching mechanism takes into account any disturbances in the system. With higher levels of noise delays the switching whereas for lower levels, the switching is triggered sooner. The algorithm is also robust to False Switching (FS) due to the MMB processing. In terms of performance, semi-adaptive has shown BF filter computing power reduction of up to 98% without degradation in system performance. The approach can pave the way for the evolution of onboard BF by reducing the energy requirements associated with interference mitigation. Although the algorithm has been proposed for a mobile-satellite scenario, the approach can be applied more widely in other systems to improve their energy efficiency.

Appendix A

Proof of β_{SA}

Proof of β_{Ψ}:

With ρ as the length of MMW, the variance Ψ can be presenting generically as:

$$\Psi_{\rho} = \frac{(\rho-1)\times\Psi_{\rho-1} + \left\{w_{\rho} - \left(\frac{1}{l}\sum_{l=1}^{\rho} w_l\right)\right\}^2}{\rho} \tag{44}$$

The complexity of (44) lies at $4M+(\rho+2)P$. For the computation of variance over all MMWs, we need to evaluate the total MMBs to be processed. As MMB moves over g OFDM symbols after $\rho \times f$ symbols have elapsed, the total MMBs during transmission of L symbols are:

$$\mid \text{MMB} \mid = \frac{L-\rho f}{g} + 1 \tag{45}$$

The complexity associated with variance computation is critically influenced by the parameter g, with $g = a\rho$ corresponding to the less complex case. The scalar relationship means that the Ψ would be computed for only a non-overlapping MMWs. Thus, β_Ψ can be presented as:

$$\begin{aligned} \beta_\Psi &= \left\{ f + \left(\frac{L-\rho f}{g} \right) \left(\frac{g}{\rho} \right) \right\} \times \{4M + (\rho+2)\, P\} \\ &= \left(\frac{L}{\rho} \right) \times \{4M + (\rho+2)\, P\} \end{aligned} \tag{46}$$

Proof of $\beta_{\nabla\Psi}$:

When considering the 1^{st} and f^{th} MMW of the 1^{st} MMB, only 1 adjacent Ψ value for gradient calculation is available. Therefore, computation lies at P for each of them. For the rest of $f-2$ MMWs, operations lie at $M+P$ as 2 adjacent values are available. Furthermore, there are overlapping MMWs for which gradient is not required to be recomputed. After the MMB slides over g symbols, the last MMW of the MMB has only one Ψ for gradient calculation whereas a have 2 adjacent Ψ values. Hence the computation for all possible MMB can be given as:

$$\beta_{\nabla\Psi} = [2P + (f-2)\{M+P\}] + \left[\left(\frac{L-f\rho}{g} \right) P + \left(\frac{L-f\rho}{\rho} \right) \{M+P\} \right] \tag{47}$$

Proof of β_s and β_Ω:

Switching can potentially take place once every MMB. Hence β_s can be given by:

$$\beta_s = \left(\frac{L-f\rho}{g} + 1 \right) P \tag{48}$$

Complexity β_Ω is directly proportional to γ_s. Hence,

$$\beta_\Omega = \gamma_s M \tag{49}$$

ACKNOWLEDGEMENT

Ammar H. Khan would like to thank Centre for Communication Systems Research, UK and National University of Sciences and Technology, Pakistan for supporting him in this work.

REFERENCES

[1] A. Khan, M. Imran, and B. Evans, "Adaptive beamforming for OFDM based hybrid mobile satellite system," in *27th ICSSC 2009, American Institute of Aeronautics and Astronautics*, Edinburgh, UK, June 2009.

[2] D. Zheng and P. D. Karabinis, "Adaptive beam-forming with interference supression in MSS with ATC," in *23rd ICSSC 2005, American Institute of Aeronautics and Astronautics*, Rome, Italy, Sep. 2005.

[3] A. Pollok, W. Cowley, and N. Letzepis, "Symbol-wise beamforming for MIMO-OFDM transceivers in the presence of co-channel interference and spatial correlation," *Wireless Communications, IEEE Transactions on*, vol. 8, no. 12, pp. 5755–5760, 2009.

[4] S. Li, D. Huang, K. Letaief, and Z. Zhou, "Multi-stage beamforming for coded OFDM with multiple transmit and multiple receive antennas," *Wireless Communications, IEEE Transactions on*, vol. 6, no. 3, pp. 959 – 969, march 2007.

[5] J. Li, K. B. Letaief, and Z. Cao, "Co-channel interference cancellation for space-time coded OFDM systems," *Wireless Communications, IEEE Transactions on*, vol. 2, no. 1, pp. 41– 49, 2003.

[6] A. H. Khan, M. A. Imran, and B. G. Evans, "OFDM based adaptive beamforming for hybrid terrestrial-satellite mobile system with pilot reallocation," *Satellite and Space Communications, 2009. IWSSC 2009. International Workshop on*, pp. 201 – 205, Sep. 2009.

[7] A. Khan, M. Imran, and B. Evans, "Preamble based adaptive beamformer for hybrid terrestrial-satellite mobile system," in *28th ICSSC 2010, American Institute of Aeronautics and Astronautics*, California, USA, Sep. 2010.

[8] ——, "Iterative turbo beamforming for OFDM based hybrid terrestrial-satellite mobile system," *Communications, IET*, proposal under review.

[9] F. Makita and K. Smith, "Design and implementation of ICO system," in *17th ICSSC 1998, American Institute of Aeronautics and Astronautics*, Yokohama, Japan, Feb. 1998.

[10] P. Angeletti and N. Alagha, "Space/ground beamforming techniques for emerging hybrid satellite terrestrial networks," *ICSSC 2009, American Institute of Aeronautics and Astronautics*, 2009.

[11] A. Draganov and A. Weinberg, "Optimized beamforming for satellite communication," *U.S. Patent 0232227 A1*, 4 Oct 2007.

[12] A. Tandon, M. N. S. Swamy, and M. O. Ahmad;, "Partial-update L_∞-norm based algorithms," *Circuits and Systems I: Regular Papers, IEEE Transactions on*, vol. 54, no. 2, pp. 411 – 419, 2007.

[13] M. Godavarti and A. Hero, "Partial update LMS algorithms," *Signal Processing, IEEE Transactions on*, vol. 53, no. 7, pp. 2382 – 2399, 2005.

[14] S. Douglas, "Adaptive filters employing partial updates," *Circuits and Systems II: Analog and Digital Signal Processing, IEEE Transactions on*, vol. 44, no. 3, pp. 209 – 216, 1997.

[15] J.-Y. Ko and Y.-H. Lee;, "Adaptive beamforming with dimension reduction in spatially correlated MISO channels," *Wireless Communications, IEEE Transactions on*, vol. 8, no. 10, pp. 4998 – 5002, 2009.

[16] L. Scott and B. Mulgrew, "Sparse LCMV beamformer design for suppression of ground clutter in airborne radar," *Signal Processing, IEEE Transactions on*, vol. 43, no. 12, pp. 2843 – 2851, 1995.

[17] ETSI TS 102 585, "System specifications for satellite services to handheld devices (SH) below 3 GHz," July 2007.

[18] P. D. Karabinis, "Systems and methods for terrestrial reuse of cellular satellite frequency spectrum," *U.S. Patent 6684057*, 27 Jan 2004.

[19] D. Slock, "On the convergence behavior of the LMS and the normalized LMS algorithms," *Signal Processing, IEEE Transactions on*, vol. 41, no. 9, pp. 2811 –2825, sep 1993.

[20] S. Douglas, "A family of normalized LMS algorithms," *Signal Processing Letters, IEEE*, vol. 1, no. 3, pp. 49 –51, mar 1994.

[21] R. Kwong and E. Johnston, "A variable step size LMS algorithm," *Signal Processing, IEEE Transactions on*, vol. 40, no. 7, pp. 1633 – 1642, July 1992.

[22] B. D. V. Veen and K. M. Buckley, "Beamforming: A versatile approach to spatial filtering," *ASSP Magazine, IEEE*, vol. 5, no. 2, pp. 4 – 24, April 1988.

[23] M. Luke and R. Reggiannini, "Carrier frequency acquisition and tracking for OFDM systems," *Communications, IEEE Transactions on*, vol. 44, no. 11, pp. 1590 – 1598, Mar 1996.

[24] M. Luise, M. Marselli, and R. Reggiannini, "Low-complexity blind carrier frequency recovery for OFDM signals over frequency-selective radio channels," *Communications, IEEE Transactions on*, vol. 50, no. 7, pp. 1182 – 1188, Jul 2002.

[25] ETSI TR 102 662, "Satellite earth stations and systems (SES); Advanced satellite based scenarios and architectures for beyond 3G systems," Mar. 2010.

FIGURES AND TABLES

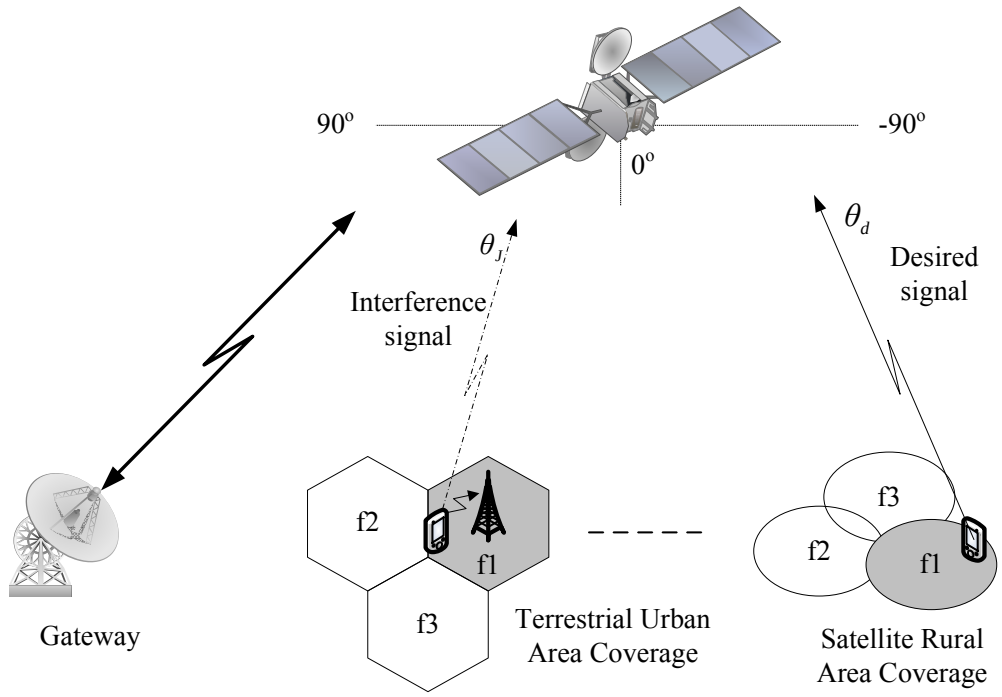

Fig. 1. Hybrid Terrestrial-Satellite Mobile System scenario

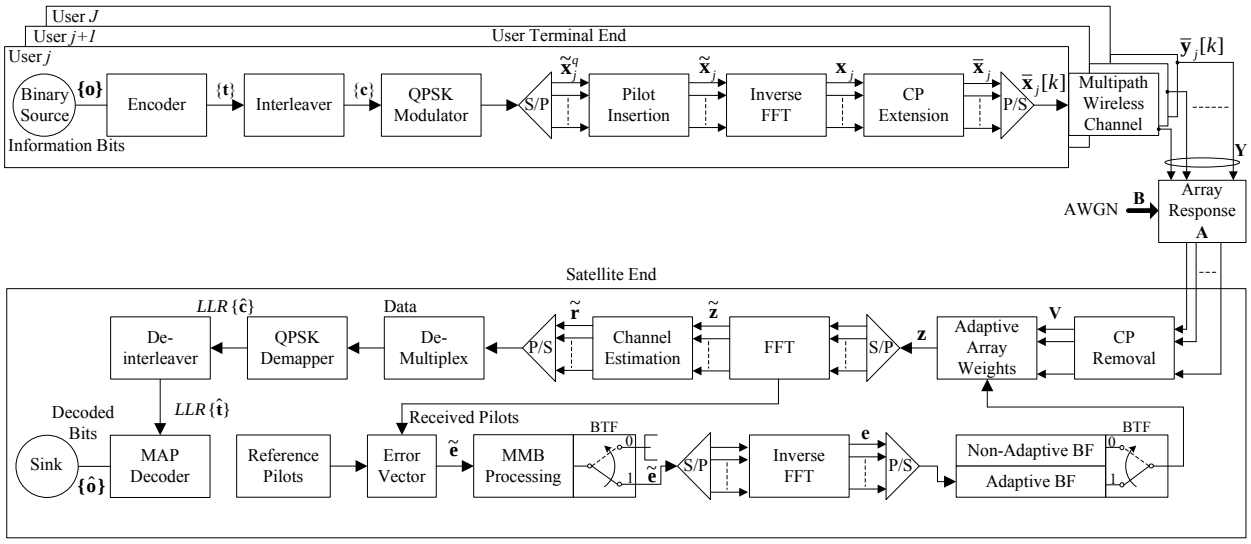

Fig. 2. HTSMS transceiver architecture with semi-adaptive beamformer

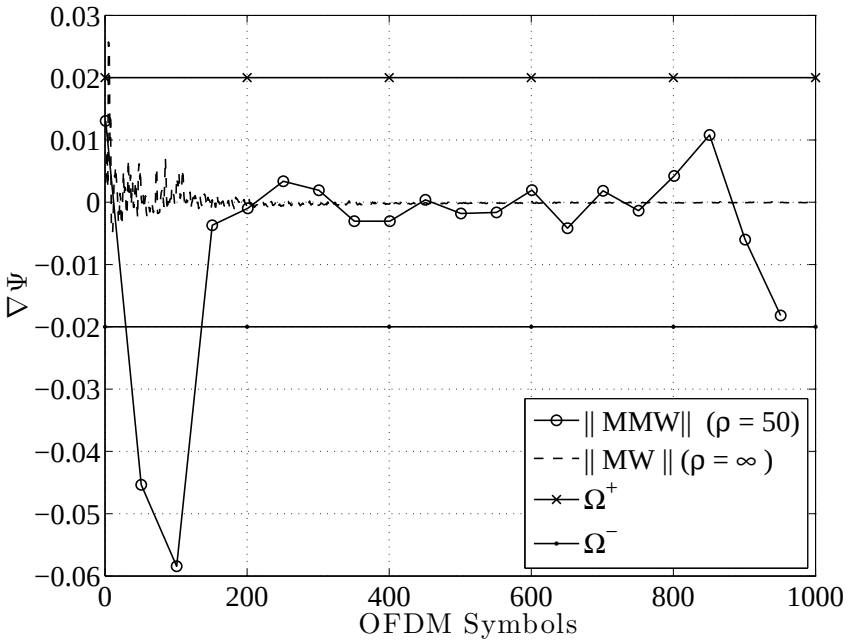

Fig. 3. $\nabla\Psi$ vs OFDM symbols with $\sigma^2 = 1$, $\rho = 50$, $g = 50$, $N = 32$, $N_p = 5$ and antenna elements $= 4$.

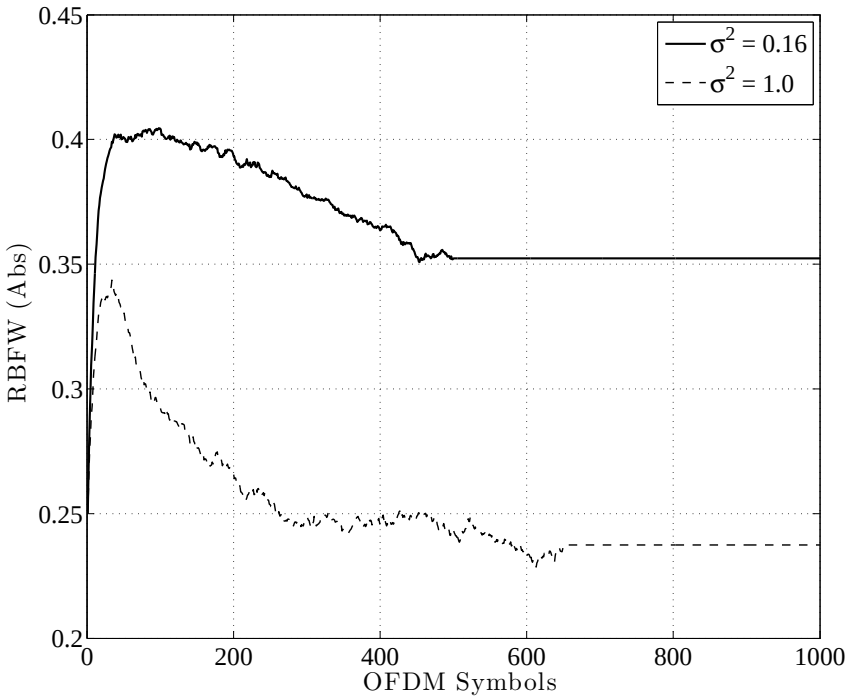

Fig. 4. Beamforming convergence in terms of Real-time Beamforming Weights (Abs) of one of the antenna elements vs OFDM symbols with $\rho = 50$, $f = 10$, $g = 50$, $\sigma^2 = 1.0$ & 0.16 and antenna elements $= 4$.

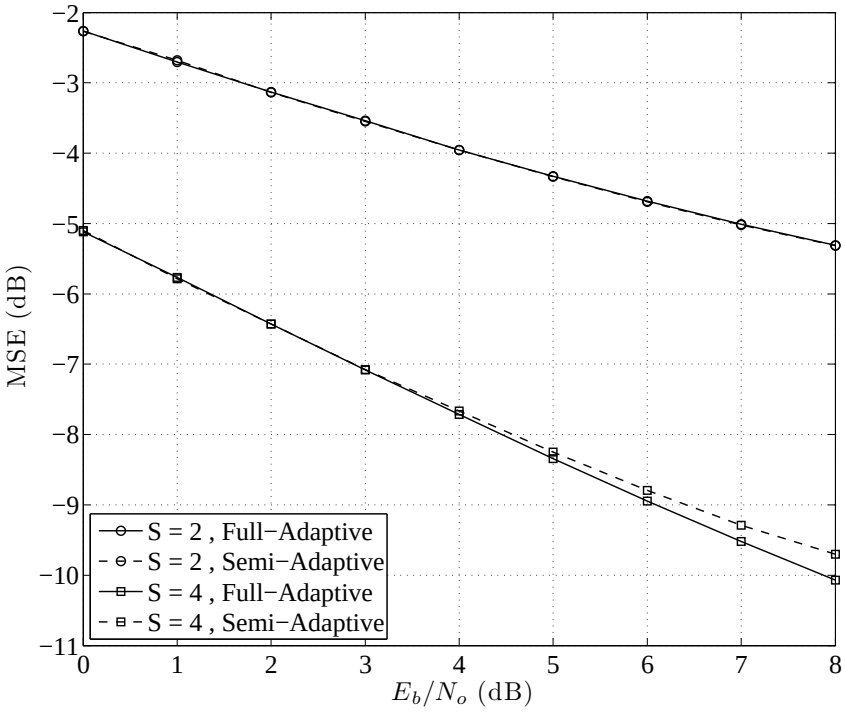

Fig. 5. Beamforming prediction error in terms of MSE vs E_b/N_o for full-adaptive and proposed semi-adaptive BF with $\rho = 50$, $f = 10$, $g = 50$ and antenna elements $= 2$ & 4.

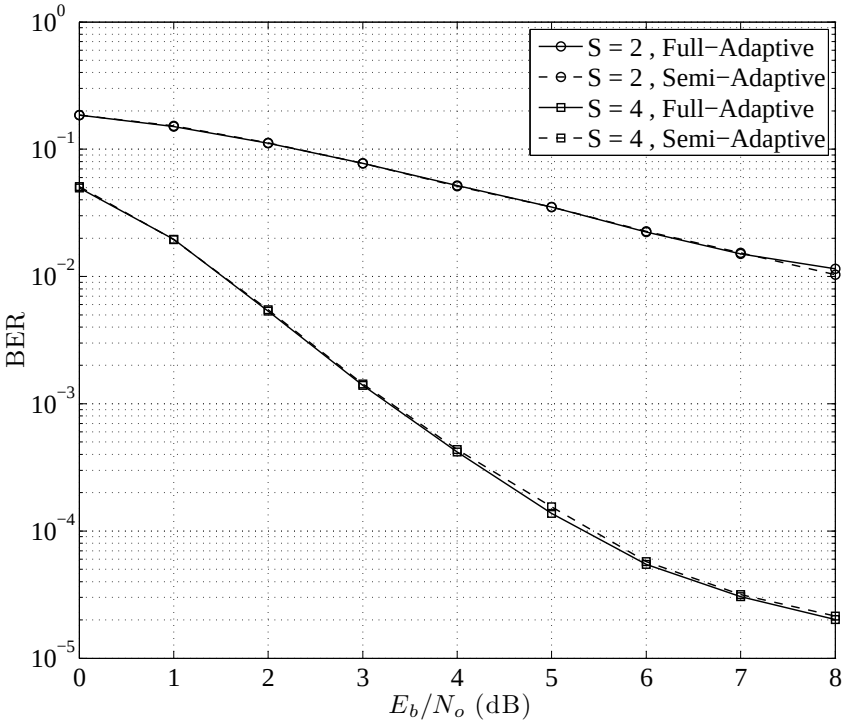

Fig. 6. Bit Error Rate vs E_b/N_o for full-adaptive and proposed semi-adaptive BF with $\rho = 50$, $f = 10$, $g = 50$ and antenna elements $= 2$ & 4.

TABLE I
SEMI-ADAPTIVE BEAMFORMING ALGORITHM

Algorithm 1 Semi-Adaptive LMS Beamforming

Initialise: $(s, l, \mu, f, g, \rho,$ MMB)

Require: Λ (BTF) $\leftarrow 1$ for $l = 1$
$\sum_{s=1}^{s=S} w(s) = 1$ for $l = 1$
$\mu_{min} \leq \mu \leq \mu_{max}$ for every l

while $l \leq L$ **do**
  input $\mathbf{e}_l$ for every l
  Compute $\nabla\Psi$ and Ω over MMB
  if $\Lambda = 1$ **and** $|\nabla\Psi| \leq |\Omega|$ **then**
    $\Lambda \leftarrow 0$
    $\mathbf{w}[l+1] = \mathbf{w}[l]$
  else if $\Lambda = 1$ **and** $|\nabla\Psi| \geq |\Omega|$
    $\Lambda[l] = \Lambda[l-1]$
    Computation of $\mathbf{w}[l+1] \Rightarrow \mathbf{w}[l]$
  else if $\Lambda = 0$ **and** $|\nabla\Psi| \geq |\Omega|$
    $\Lambda \leftarrow 1$
    $\mathbf{w}[l+1] = \mathbf{w}[l] + \mu e[l]\mathbf{x}[l]$
  else
    $\Lambda[l] = \Lambda[l-1]$
    Computation of $\mathbf{w}[l+1] \Rightarrow \mathbf{w}[l]$
  end if
  Move MMB over g OFDM symbols
end while

TABLE II
MSS PARAMETERS

Carrier Data	
Code Rate	$\frac{1}{2}$
Filler Roll-Off	25%
Modulation	QPSK
Transmission overhead	10%
Downlink Data	
EIRP per carrier	35 dB
Free Space Loss	195 dB
Pointing Loss	0.5 dB
Rain Loss	6 dB
Earth Station G/T	35 dB
System Temperature	120° K
Implementation Margin	3 dB
Intermodulation Interference	1 dB
ICI due to CFO	$1/3$ dB

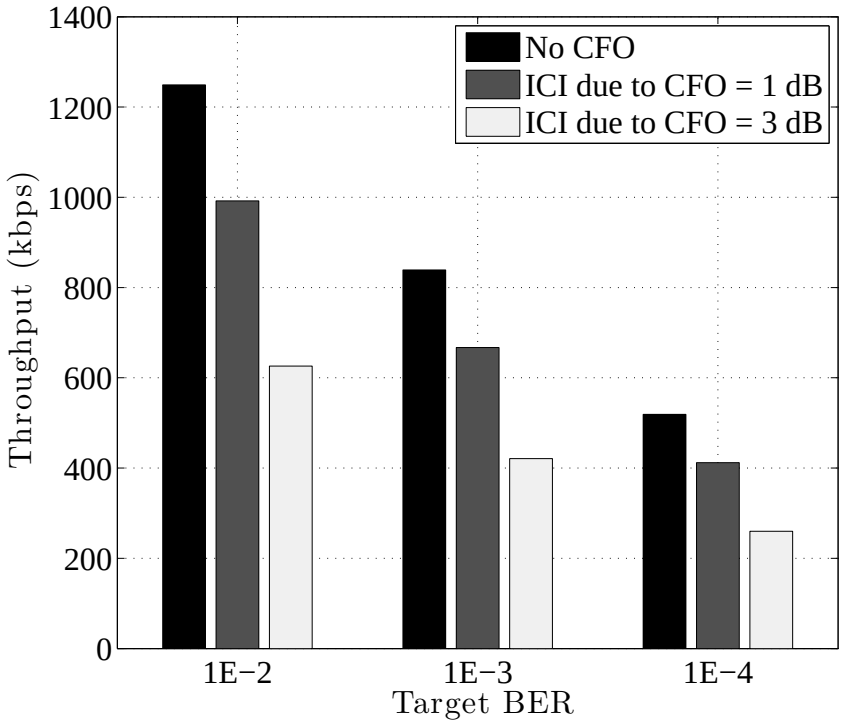

Fig. 7. Throughput comparison for different target Bit Error Rates with and without CFO in the system.

TABLE III
MAESTRO CHANNEL PARAMETERS - OUTDOOR RURAL

Tap Index	Delay [ns]	Power Loss [dB]
1	0	91.9
2	195.3	106.3
3	260.4	110.1
4	846.3	112.5
5	1171.9	110.2
6	1953.1	112.5
7	2734.3	112.5

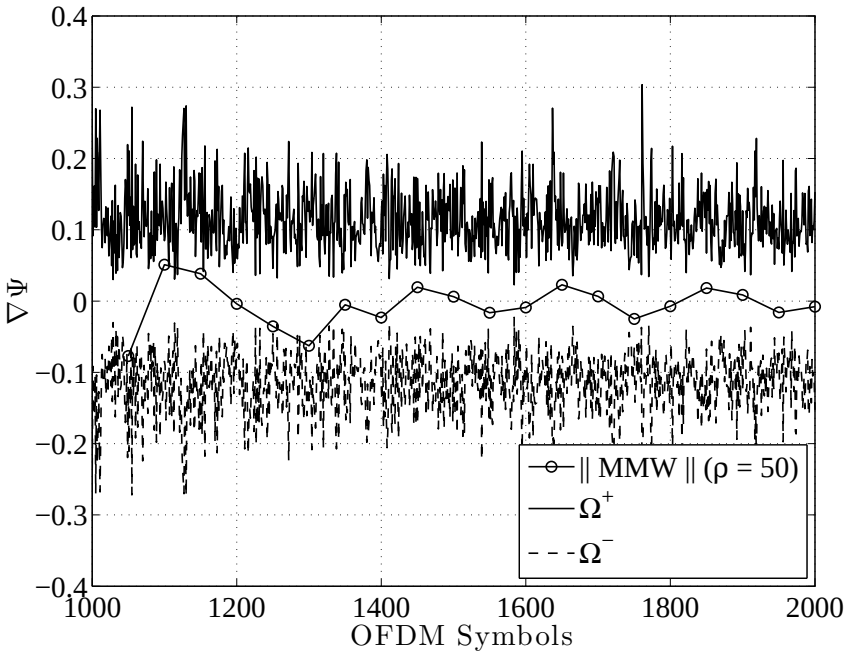

Fig. 8. $\nabla\Psi$ vs OFDM symbols with $L_c = 1000$, $\sigma^2 = 0.1$, $\rho = 50$, $g = 50$, $N = 32$, $N_p = 5$ and antenna elements $= 4$.

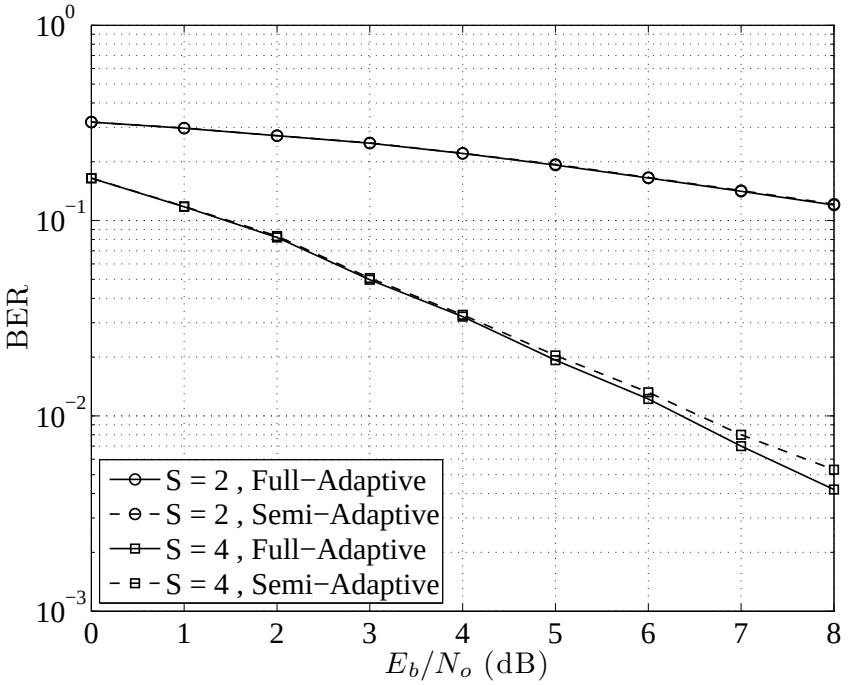

Fig. 9. Bit Error Rate vs E_b/N_o for Rural case with mobile speed $= 3$ km/hr, $L_c = 1000$, $\rho = 50$, $f = 3$, $g = 50$ and antenna elements $= 2$ & 4.